PNAS RESEARCH ARTICLE | CELL BIOLOGY

An unanticipated discourse of HB-EGF with VANGL2 signaling during embryo implantation

Yeon Sun Kim[a], Jia Yuan[a,1], Amanda Dewar[a], Jean-Paul Borg[b,c], David W. Threadgill[d], Xiaofei Sun[a,2], and Sudhansu K. Dey[a,2]

Edited by Thomas Spencer, University of Missouri, Columbia, MO; received February 22, 2023; accepted April 13, 2023

Implantation is the first direct encounter between the embryo and uterus during pregnancy, and *Hbegf* is the earliest known molecular signaling for embryo–uterine crosstalk during implantation. The downstream effectors of heparin-binding EGF (HB-EGF) in implantation remain elusive due to the complexity of EGF receptor family. This study shows that the formation of implantation chamber (crypt) triggered by HB-EGF is disrupted by uterine deletion of *Vangl2,* a key planar cell polarity component (PCP). We found that HB-EGF binds to ERBB2 and ERBB3 to recruit VANGL2 for tyrosine phosphorylation. Using in vivo models, we show that uterine VAGL2 tyrosine phosphorylation is suppressed in *Erbb2/Erbb3* double conditional knockout mice. In this context, severe implantation defects in these mice lend support to the critical role of HB-EGF-ERBB2/3-VANGL2 in establishing a two-way dialogue between the blastocyst and uterus. In addition, the result addresses an outstanding question how VANGL2 is activated during implantation. Taken together, these observations reveal that HB-EGF regulates the implantation process by influencing uterine epithelial cell polarity comprising VANGL2.

Vangl2 | HB-EGF | ERBBs | planar cell polarity | pregnancy

Embryo implantation is central to pregnancy success (1). A reciprocal interaction between an implantation-competent blastocyst and a receptive uterus is critical to successful implantation. In mice, embryos enter the uterus early on day 4 morning (day 1 = vaginal plug). The initial attachment reaction occurs on day 4 evening (2,000 to 2,400 h) at the antimesometrial pole of the uterus (2). Normally, embryos are well positioned in an implantation chamber (crypt) in the uterine lumen to initiate a crosstalk between the two entities. The attachment reaction triggers stromal cell decidualization, with the disappearance of the crypt epithelium through entosis (3). A healthy crypt is critical for implantation and pregnancy success. We showed that the *Wnt5a*-Ror (Receptor Tyrosine Kinase Like Orphan Receptors)-planar cell polarity (PCP) signaling pathway governs crypt formation (4, 5). The disruption of noncanonical *Wnt5a* signaling in mice with uterine loss or gain of function of *Wnt5a* or loss of function of its coreceptors, *Ror1* and *Ror2*, results in aberrant crypt formation, embryo spacing, and defective implantation. PCP is a downstream target of the noncanonical *Wnt5a* signaling, controlling cell movement and organ morphogenesis. Uterine cell-specific deletion of Vang-like protein 2 (*Vangl2*), a major component of PCP signaling, impairs formation of crypts, embryo spacing, and decidualization, compromising pregnancy outcomes (4). The blastocyst initiates a two-way communication several hours before the attachment reaction occurs. Heparin binding EGF (HB-EGF-like growth factor encoded by *Hbegf*) first appears in epithelial cells juxtaposed with blastocysts around 1,600 to 1,800 h on day 4 of pregnancy. Systemic and conditional deletion of *Hbegf* by progesterone receptor (*Pgr*)-Cre shows reproductive deficiencies in mice (6). Furthermore, blastocyst-size sepharose blue beads loaded with HB-EGF transferred to day 4 pseudopregnant uteri can trigger implantation-like changes similar to those seen in normal pregnancy (7). HB-EGF executes its function via transmembrane (TM) EGF family of receptors (ERBBs 1-4) as homodimers or heterodimers and induces autophosphorylation on tyrosine residues (8, 9). They share a common structural feature but differ in their ligand affinity and kinase activity. ERBB2, which is thought to lack a direct ligand, possesses the strongest kinase activity and is a preferred partner in forming dimers with other family members (9). In contrast, ERBB3 exhibits impaired kinase activity and requires heterodimerization with other receptor subtypes for intracellular signaling (10–12). While EGF, Transforming growth factor alpha, HB-EGF, amphiregulin (AREG), betacellulin, and epiregulin can directly bind to ERBB1, all neuregulins (NRGs) require either ERBB3 or ERBB4 for direct binding. Additionally, betacellulin, HB-EGF, and epiregulin can serve as direct ligands for ERBB4. However, the exact roles of different EGF family of receptors and downstream effectors in the crypt formation are not clear.

Significance

Healthy embryo implantation is a gateway to pregnancy success. Here we show a unique dialogue between HB-EGF and VANGL2 in implantation. HB-EGF and *Vangl2* are expressed in the uterus around implantation. Limited pregnancy success in the absence of HB-EGF and VANGL2 signifies their importance in implantation. Beads preloaded with HB-EGF if transferred into pseudopregnant uteri elicit implantation-like responses that are muted in *Vangl2* deleted uteri. We found that HB-EGF, ERBB2, ERBB3, and VANGL2 have physical interactions, leading to VANGL2 tyrosine phosphorylation. This event fails to occur in uteri deficient of both ERBB2 and ERBB3. Severe implantation defects in these double mutant mice simulate those seen in *Vangl2* mutants, suggesting a close intimacy of HB-EGF with VANGL2 tyrosine phosphorylation in implantation.

Author contributions: Y.S.K., J.Y., X.S., and S.K.D. designed research; Y.S.K., J.Y., A.D., and X.S. performed research; J.-P.B. and D.W.T. contributed new reagents/analytic tools; Y.S.K., X.S., and S.K.D. analyzed data; and Y.S.K., X.S., and S.K.D. wrote the paper.

The authors declare no competing interest.

This article is a PNAS Direct Submission.

[1]Present address: Department of Cell Biology, Advanced Medical Research Institute, Cheeloo College of Medicine, Shandong University, Jinan, Shandong province 250100, China.

[2]To whom correspondence may be addressed. Email: Xiaofei.sun@cchmc.org or sk.dey@cchmc.org.

This article contains supporting information online at https://www.pnas.org/lookup/suppl/doi:10.1073/pnas.2302937120/-/DCSupplemental.

Published May 8, 2023.

Beads carrying HB-EGF fail to form crypts in *Vangl2*-deleted uteri (5), suggesting a dialogue between VANGL2 and HB-EGF. We show here that ERBBs physically interact with VANGL2. In particular, VANGL2 physically interacts with ERBB2, ERBB3 and ERBB4, but not ERBB1. Tyrosine kinase domains in ERBBs undergo auto-phosphorylation upon ligand activation which in turn can trans-phosphorylate other proteins. We show here that HB-EGF can induce tyrosine phosphorylation of VANGL2 through ERBB2 and ERBB3 heterodimers. To study whether the tyrosine phosphorylation requires ERBB2/3 dimerization in vivo, we generated a mouse line with uterine conditional deletion of both *Erbb2* and *Erbb3* by crossing them with $Pgr^{cre/+}$ mice ($Erbb2/3^{d/d}$). We found that VANGL2 tyrosine phosphorylation is abolished in $Erbb2/3^{d/d}$ uteri in response to HB-EGF. In addition, $Erbb2/3^{d/d}$ double conditional knockout (cKO) mice like $Vangl2^{d/d}$ females show severe subfertility.

Results

HB-EGF Fails to Form Crypts-Like Structures in $Vangl2^{f/f};Ltf^{cre/+}$ Mice. *Hbegf* is exclusively expressed in the crypt epithelium around blastocysts 6 to 7 h before the initiation of implantation (blue bands) (13, 14), and important for implantation. HB-EGF-carrying beads transferred to day 4 pseudopregnant mice induce appropriate gland-crypt assembly, establishing a direct communication between the glands and the embryo. This landscape is orchestrated by VANGL2 signaling. To examine whether HB-EGF can overcome uterine epithelial deficiency in *Vangl2*, we generated $Vangl2^{f/f}$;Lactoferrin ($Ltf)^{cre/+}$ ($Vangl2^{ed/ed}$) mice, in which epithelial *Vangl2* is efficiently deleted in the adult uterus (5).

Blastocyst-size Affi-Gel blue beads loaded with HB-EGF were transferred into day 4 pseudopregnant $Vangl2^{ed/ed}$ uteri (5, 7). Mice were killed 48 h later, and implantation-like responses were demarcated by the blue dye method. Using tissue clearing and three dimensional (3D) imaging, we show that HB-EGF-carrying beads trigger gland-crypt–like assembly in $Vangl2^{f/f}$ pseudopregnant mice but not in $Vangl2^{ed/ed}$ counterparts (Fig. 1), indicating that VANGL2 functions downstream of HB-EGF.

ERBB2, ERBB3, and HB-EGF Have Direct Protein–Protein Interactions with VANGL2. HB-EGF triggers gland-crypt assembly in wildtype (WT) mice, which requires PCP signaling in the uterus. However, the underlying mechanism of interactions between HB-EGF and PCP signaling remains elusive. Therefore, we examined whether HB-EGF or members of the ERBB receptors directly and physically interact with VANGL2 signaling. AREG, progesterone (P_4)-regulated growth factor in the HB-EGF family, was also evaluated for VANGL2 interaction. Previously we showed AREG, but not epiregulin, partially compensates for HB-EGF's deficiency in female reproduction (6).

We labeled ERBB1-4, as well as HB-EGF and AREG with hemagglutinin (HA) tags, thus designated ERBB1-HA, ERBB2-HA, ERBB3-HA, ERBB4-HA, HB-EGF-HA, and AREG-HA vectors. To explore ERBBs' interaction with VANGL2, we co-transfected HA-tagged vectors with a VANGL2-Flag vector into 239T cells. VANGL2 was pulled down using an anti-Flag antibody. We observed that VANGL2 physically interacts with ERBB2, ERBB3, and ERBB4, but not ERBB1 (Fig. 2 *A*–*C* and *SI Appendix*, Fig. S1*A*). We also found that HB-EGF, but not AREG, shows physical association with VANGL2 (Fig. 2*D* and *SI Appendix*, Fig. S1*B*).

We have previously shown that *Erbb2* and *Erbb3* are primarily expressed in the uterine epithelium on day 4 of pregnancy, whereas *Erbb4* is expressed in blastocysts, sub-myometrial stroma and myometrial connective tissues. On day 5, *Erbb2* and *Erbb3* are expressed in the epithelium and stroma at the implantation site and on day 8, in the decidual zone (15–17). VANGL2 shows a similar expression pattern as those of *Erbb2* and *Erbb3* (4, 5). To further investigate the association in vivo, co-immunoprecipitation (Co-IP) experiments were conducted using day 4 endometrial protein lysates. The results confirmed the physical interaction of VANGL2 with ERBB2 and ERBB3, but not with ERBB1 (Fig. 3 *A*–*D*). ERBB2 and ERBB3 form a heterodimer in $Erbb2^{f/f}$ uteri (Fig. 3*E*). However, the interaction between VANGL2 and ERBB3 was absent in $Erbb2^{d/d}$ endometrial protein lysates (Fig. 3*F*), suggesting ERBB3 is tethered to the complex via ERBB2. This is

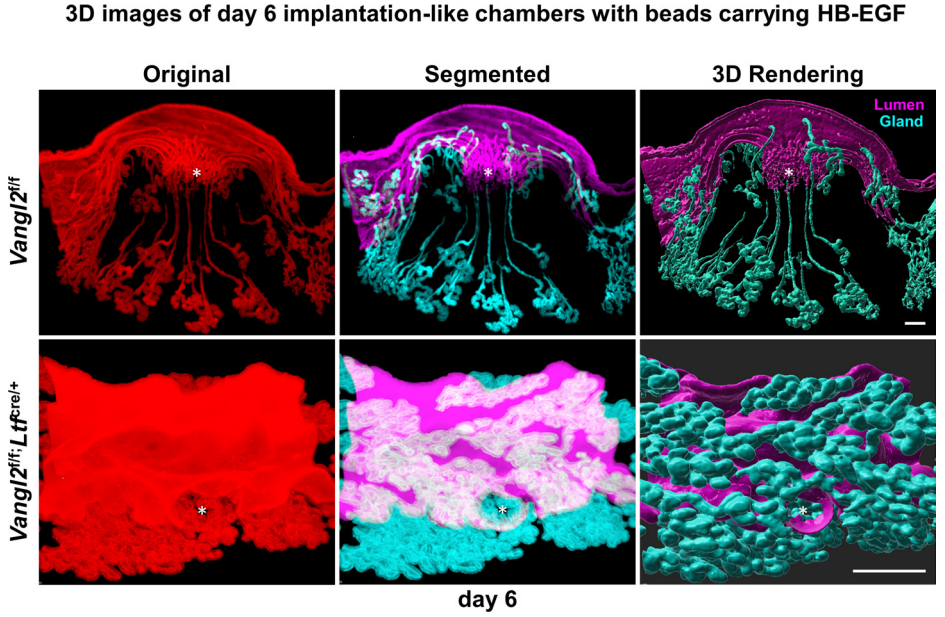

Fig. 1. 3D images of day 6 implantation-like chambers with beads carrying HB-EGF. 3D images show that HB-EGF-carrying beads, similarly transferred into day 4 pseudopregnant uteri of $Vangl2^{f/f};Ltf^{cre/+}$ mice cannot trigger gland-crypt like responses on day 6. Single-layer images show the bead positions in the uterus. Asterisks (*) indicate the location of beads. (Scale bar, 200 μm.)

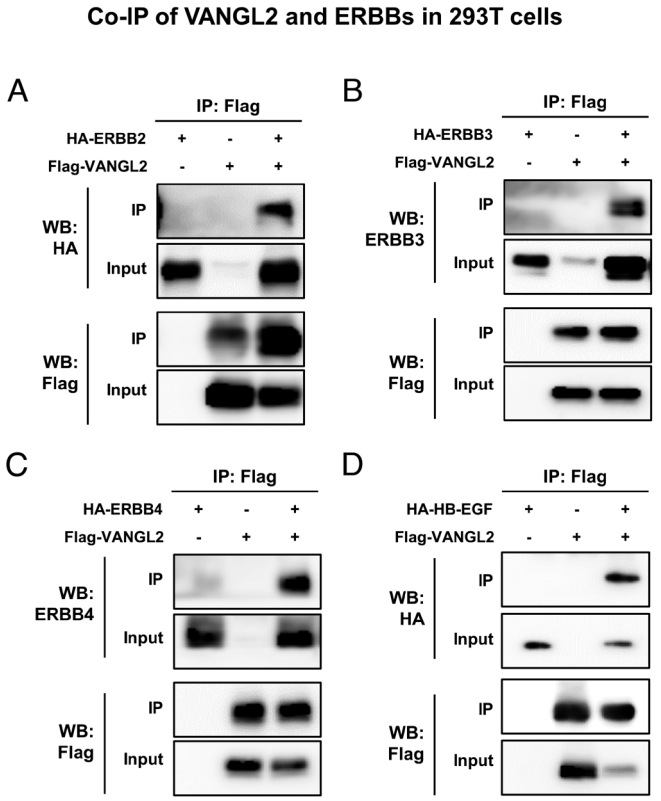

Fig. 2. Co-IP of VANGL2 and ERBBs in 293T Cell Protein Lysates. (*A–D*) 4XFlag-VANGL2 vector co-transfected with ERBB2-HA, ERBB3-HA, ERBB4-HA, and HA-HB-EGF into 293T cells. The protein lysates were immunoprecipitated (IP) with the anti-Flag antibody, followed by WB with anti-HA, anti-ERBB3, anti-ERBB4 and anti-Flag antibodies.

similar to the finding that the ERBB2/ERBB3 dimer functions as an oncogenic mover for breast cancer cell proliferation (18). Taken together, these results suggest that ERBB2 forms a protein complex with ERBB3 and VANGL2.

TM and C-Terminal Domains of VANGL2 Directly Interact with ERBB2/3. To examine which domains of VANGL2 interact with ERBB2 or ERBB3, we generated truncated fragments of VANGL2 with Flag tags: N-terminal (N)-VANGL2-Flag, TM-VANGL2-Flag, C-terminal (C)-VANGL2-Flag as well as deletion of N (ΔN)-VANGL2-Flag and deletion of C (ΔC)-VANGL2-Flag constructs (Fig. 4*A*). These constructs were transfected in 293T cells for Co-IP experiments. These results show that segments containing the TM and C-terminal domain of VANGL2 physically interact with ERBB2 and ERBB3 (Fig. 4 *B* and *C*).

HB-EGF Induces Tyrosine Phosphorylation of VANGL2 in Madin–Darby Canine Kidney (MDCK) Cells and Day 4 Uteri Via ERBBs. Our results showing HB-EGF's interaction with VANGL2 to direct implantation chamber (crypt) formation (5) led us to explore how HB-EGF interfaces with VANGL2 signaling. The mechanism by which VANGL2 is activated is largely unknown and a ligand has yet to be discovered that directly activates VANGL2. A previous report shows that VANGL2 is activated by phosphorylation on serine/threonine residues (19). VANGL2 signaling can direct organized cell movement, and thus VANGL2 phosphorylation may well be participating in this action. Given *Vangl2*'s association with receptor tyrosine kinases (Figs. 2 and 3), it is conceivable that VANGL2 also undergoes tyrosine phosphorylation by ERBBs following exposure to HB-EGF.

MDCK cells are polarized (20, 21) and express VANGL2 and ERBBs (*SI Appendix*, Fig. S2). To study potential phosphorylation changes of VANGL2 by HB-EGF, we performed kinase-IP assays. MDCK cell protein lysates (200 μg) were treated with HB-EGF (150 ng) at different time points. An anti-phosphotyrosine (anti-pTyr) antibody was used to pull down tyrosine phosphorylated proteins. Western blotting (WB) results show that HB-EGF triggers VANGL2 tyrosine phosphorylation after 10 min of treatment and peaks at 50 min (Fig. 5*A*). AREG, another HB growth factor of the EGF family, is unable to associate physically with VANGL2 and fails to stimulate VANGL2 tyrosine phosphorylation (*SI Appendix*, Fig. S3), although it can partially replace HB-EGF for implantation in systemic *Hbegf* knockout females (6). As expected, HB-EGF also triggers tyrosine phosphorylation of ERBB1, ERBB2, and ERBB3 (Fig. 5*A*). These in vitro kinase-IP experiments provide evidence for interactions between VANGL2 and ERBBs leading to VANGL2 transphosphorylation via HB-EGF.

Next, we performed experiments to study whether endogenous VANGL2 in the uterine endometrium undergoes tyrosine phosphorylation prior to implantation. The implantation chamber begins to form on day 4 evening after HB-EGF expression has been initiated (14). The finding that VANGL2 phosphorylation occurs in the uterus will provide further evidence to better understand how HB-EGF helps forming an implantation chamber by collaborating with PCP signaling.

Day 4 *Vangl2*$^{f/f}$ and *Vangl2*$^{f/f}$;*Pgr*$^{cre/+}$ (*Vangl2*$^{d/d}$) pregnant uteri were slit open longitudinally and the endometria were scraped off with a blunt scalpel blade without the myometrium. Endometrial protein lysates were challenged with HB-EGF (150 ng) for 10, 20, 30 and 50 min, and an anti-pTyr antibody was used to pull down tyrosine-phosphorylated proteins. WB results show a phosphorylated VANGL2 band after 10 min of treatment in *Vangl2*$^{f/f}$ uteri. This band was not present in *Vangl2*$^{d/d}$ uteri (Fig. 5*B*).

VANGL2 TM Domain Interacts with ERBBs for VANGL2 Tyrosine Phosphorylation Following HB-EGF Exposure. We further investigated the tyrosine phosphorylation sites of VANGL2 by evaluating the two predicted tyrosine phosphorylation sites at the N-terminal of VANGL2 (https://www.phosphosite.org/homeAction). We transfected various constructs of truncated VANGL2 in 239T cells in culture. Deletion of the N-terminal (ΔN) resulted in little or no tyrosine phosphorylation, as compared to full-length VANGL2 with distinct tyrosine phosphorylation after being challenged with HB-EGF (Fig. 6*A*). Surprisingly, deletion of the C-terminal showed increased phosphorylation. These results suggest that the TM domain is critical for tyrosine phosphorylation in the N-terminal domain by HB-EGF. Next, we studied the potential phosphorylation sites on tyrosine residues after HB-EGF treatment. We generated point mutations in VANGL2 constructs by replacing each potential tyrosine residue with an alanine residue and tested each vector in the 293T cells respectively. Kinase-IP results show that VANGL2-mutation at Tyrosine7 (MutY7) and VANGL2-full length (F) constructs undergo tyrosine phosphorylation; mutation of Tyrosine10 of (MutY10) shows no Tyr-phosphorylated band (Fig. 6*B*), suggesting that Tyrosine10 is a major phosphorylation site.

Tyrosine Phosphorylation of VANGL2 Is Stifled in the Absence of Both ERBB2 and ERBB3. To confirm that VANGL2 tyrosine phosphorylation requires ERBB2 and ERBB3, we suppressed expression of *Erbb2* and/or *Erbb3* with small interfering RNAs (siRNAs) in 239T cells transfected with Flag-VANGL2 constructs. 293T cells protein lysates were challenged with HB-EGF (150 ng) for 10, 20, 30 and 50 min and an anti-pTyr antibody was used

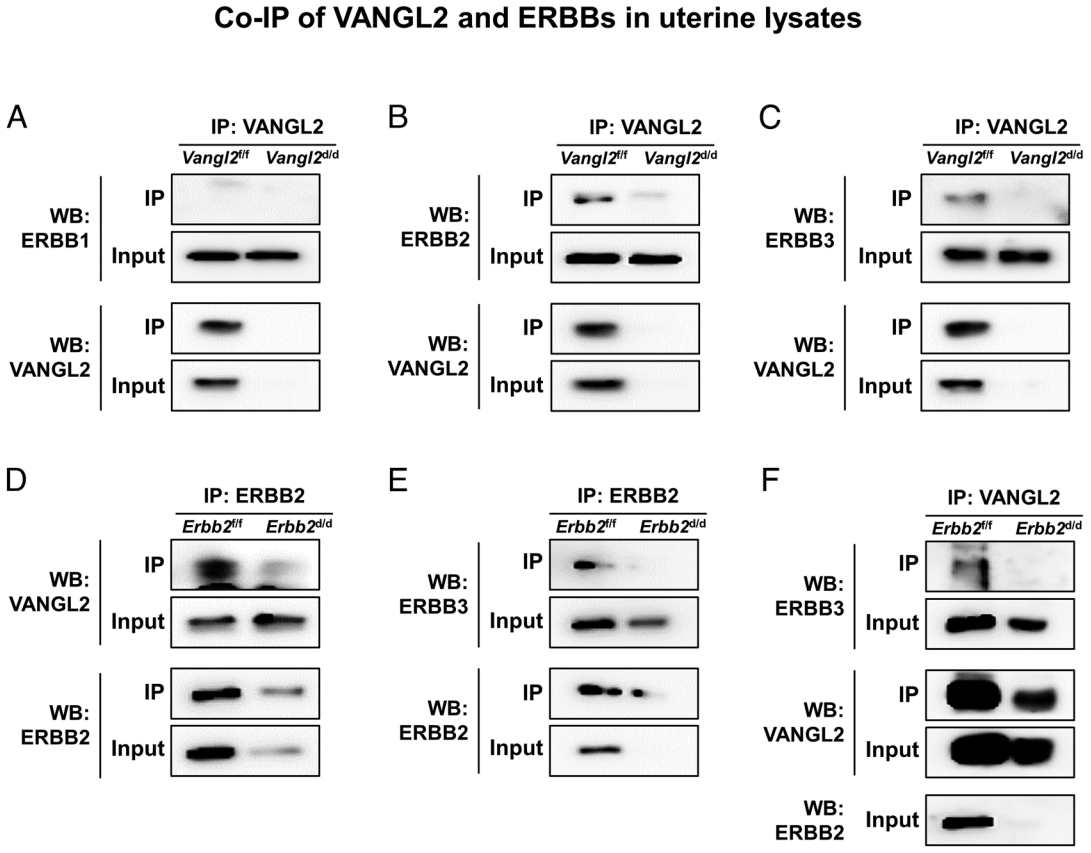

Fig. 3. Co-IP of VANGL2 and ERBBs in Endometrial Protein Lysates. (*A–C*) Protein lysates (200 μg) of *Vangl2*$^{f/f}$ or *Vangl2*$^{d/d}$ endometria of day 4 pregnant mice were immunoprecipitated (IP) with anti-VANGL2 antibody, followed by WB with anti-ERBB1, anti-ERBB2, anti-ERBB3 and anti-VANGL2 antibodies. (*D–F*) Protein lysates (200 μg) of *Erbb2*$^{f/f}$ or *Erbb2*$^{d/d}$ endometria of day 4 pregnant mice were immunoprecipitated with anti-ERBB2 antibody, followed by WB with anti-ERBB2, anti-ERBB3 and anti-VANGL2 antibodies.

to pull-down tyrosine phosphorylated proteins. Remarkably, tyrosine phosphorylation of VANGL2 is absent only when both *Erbb2* and *Erbb3* were neutralized by siRNA (Fig. 7*A*), suggesting the necessity to suppress both receptors to disrupt VANGL2 tyrosine phosphorylation. These results prompted us to generate conditional *Erbb2*/*Erbb3* double knockout mice.

Functional Coupling of HB-EGF and VANGL2 Signaling Requires the Presence of Uterine *Erbb2* and/or *Erbb3*. Since the tyrosine phosphorylation of VANGL2 depends on either *Erbb2* and/or *Erbb3*, we speculate that HB-EGF-induced tyrosine kinase activity is triggered by ERBB2 and/or ERBB3 homo- or heterodimer formation. We explored this interaction in vivo using mice

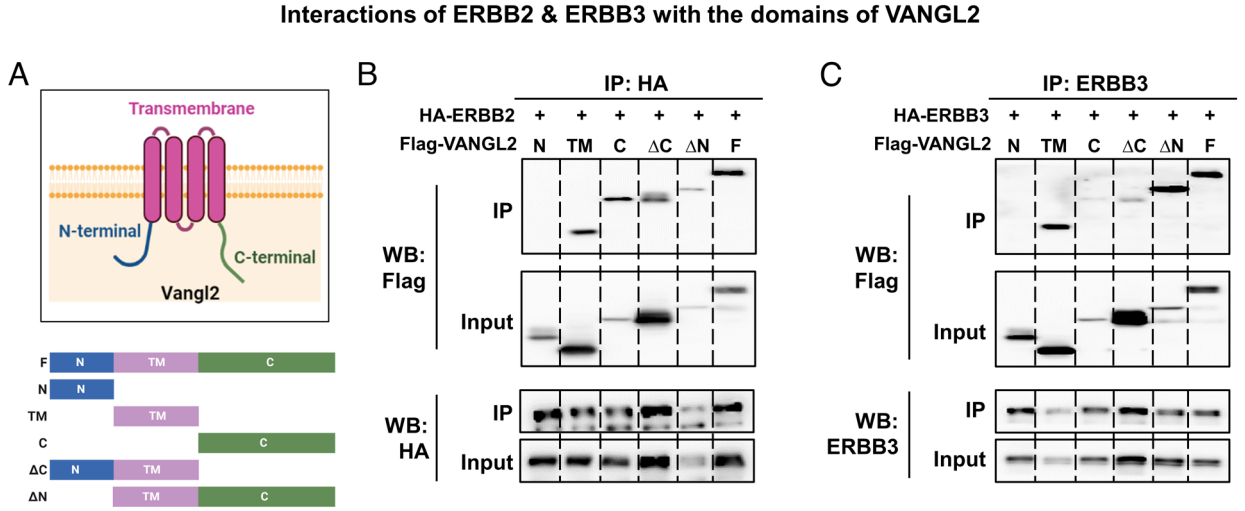

Fig. 4. Interactions of ERBB2/3 with the Domains of VANGL2. (*A*) Diagram of VANGL2 protein structure (https://biorender.com). (*B* and *C*) Flag tagged VANGL2 truncated mutant vectors co-transfected with HA-ERBB2 or HA-ERBB3 in 293T cells. C-terminal and TM of VANGL2 have physical interactions with ERBB2, but ERBB3 interacts only with TM of VANGL2. N: N-terminal; C: C-terminal; TM: TM domain; ΔC: C-terminal deleted (N + TM); ΔN: N-terminal deleted (C + TM); F: Full length.

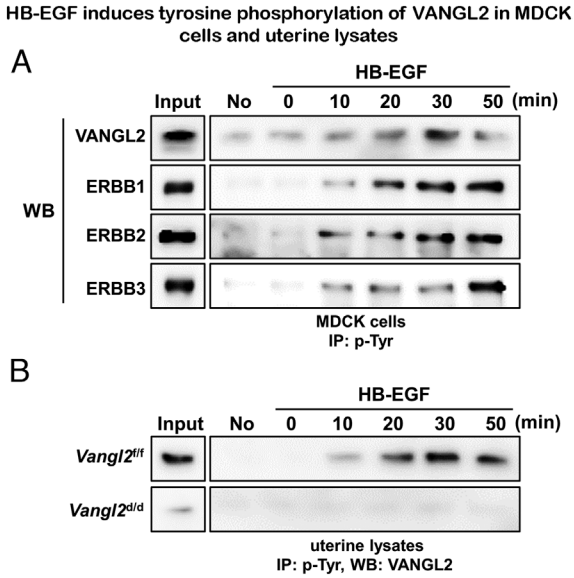

Fig. 5. HB-EGF induces tyrosine phosphorylation of VANGL2 in MDCK cells and endometrial protein lysates. (*A*) Protein lysates of MDCK cells (200 µg) were treated with HB-EGF (150 ng) for different periods. The protein lysates were immunoprecipitated (IP) with an anti-p-Tyr antibody, followed by WB with antibodies to VANGL2, ERBB1, ERBB2 and ERBB3. The results show that a VANGL2 phosphorylated band for HB-EGF is seen at 10 min with a decreased signal at 50 min. (*B*) Protein lysate (150 µg) of endometria pooled from six mice on day 4 and challenged with HB-EGF (150 ng) for different periods. The lysates were immunoprecipitated with an anti-pTyr antibody followed by WB with an anti-VANGL2 antibody.

deleted of uterine or uterine epithelial *Erbb2* and/or *Erbb3*. This was achieved by crossing *Erbb2* and/or *Erbb3* floxed mice with *Pgr-Cre* or *Ltf-Cre* mice (*Erbb2*$^{f/f}$;*Pgr*$^{cre/+}$, *Erbb2*$^{d/d}$; *Erbb3*$^{f/f}$;*Pgr*$^{cre/+}$, *Erbb3*$^{d/d}$; *Erbb2/3*$^{f/f}$;*Pgr*$^{cre/+}$, *Erbb2/3*$^{d/d}$; *Erbb2*$^{f/f}$; *Ltf*$^{cre/+}$, *Erbb2*$^{ed/ed}$; *Erbb3*$^{f/f}$;*Ltf*$^{cre/+}$, *Erbb3*$^{ed/ed}$; *Erbb2/3*$^{f/f}$;*Ltf*$^{cre/+}$, *Erbb2/3*$^{ed/ed}$). We examined litter sizes in these females. Only about 30% of both *Erbb3*$^{d/d}$ and *Erbb2/3*$^{d/d}$ plug-positive females give birth to live progeny, and *Erbb2*$^{d/d}$ and *Erbb2/3*$^{d/d}$ have significantly small litter sizes (*SI Appendix*, Table S1). However, *Erbb2*$^{ed/ed}$, *Erbb3*$^{ed/ed}$, and *Erbb2/3*$^{ed/ed}$ females show normal reproductivity. This discrepancy is likely to be due to the expression of ERBB2, ERBB3, and VANGL2 in the stroma which might have roles in implantation (4, 15, 16). Given these reproductive results, Erbb*2/3*$^{d/d}$ females with deletion of ERBB2/3 in both epithelia and stroma are used for further VANGL2 phosphorylation assays. Similar to in vitro results, VANGL2 tyrosine phosphorylation is eliminated only in *Erbb2/3*$^{d/d}$ uteri in response to HB-EGF (Fig. 7*B*). In this respect, we have recently shown that approximately 46% of plug-positive *Vangl2*$^{d/d}$ females fail to produce any litters, and the remaining 54% of plug-positive *Vangl2*$^{d/d}$ females have significantly small litters (4). Therefore, the reproductive phenotypes of *Erbb2*$^{d/d}$, *Erbb3*$^{d/d}$ and *Erbb2/3*$^{d/d}$ females are similar to that of *Vangl2*$^{d/d}$ females.

Characteristics of Implantation Defects in *Erbb2/3*$^{d/d}$ Females Are Reminiscent of those Seen in *Vangl2*$^{d/d}$ Dams. To explore the process of implantation, we first examined the vascular permeability response at the site of blastocyst attachment as assessed by an intravenous blue dye injection on day 5 of pregnancy (22). We observe that the intensity of localized blue reaction (indicative of early implantation) is uniform throughout the floxed uterus. In contrast, intensity and area of blue reactions are quite variable within the same uterine horn of *Erbb3*$^{d/d}$ and *Erbb2/3*$^{d/d}$ females (Fig. 7*C*). We also found that while the stromal cell proliferation, as assessed by Ki67 immunostaining, surrounding the blastocyst at the implantation site is robust in floxed mice, this response is sparse in *Erbb3*$^{d/d}$ with further muted in *Erbb2/Erbb3*$^{d/d}$ mice (Fig. 7*D*).

Implantation deficiencies in *Erbb2/3*$^{d/d}$ females are exemplified by very small roundish implantation chambers (crypts) as opposed to spear-shaped crypts in floxed females. Furthermore, the expression of *Ptgs2* and *Bmp2* is crucial for embryo implantation and decidualization, respectively, and serve as reliable markers of these processes (23, 24). Similar to *Vangl2*$^{d/d}$ females (4), the expression of *Ptgs2* is decreased around *Erbb2/3*$^{d/d}$ implantation chambers, but its levels are comparable in *Erbb3*$^{d/d}$ and control implantation sites (Fig. 7*E*). With the initiation of implantation, stromal cell decidualization ensues with the expression of *Bmp2*. The domains and intensities of *Bmp2* signals are significantly reduced in both *Erbb3*$^{d/d}$ and *Erbb2/3*$^{d/d}$ stromal cells as compared to control counterparts

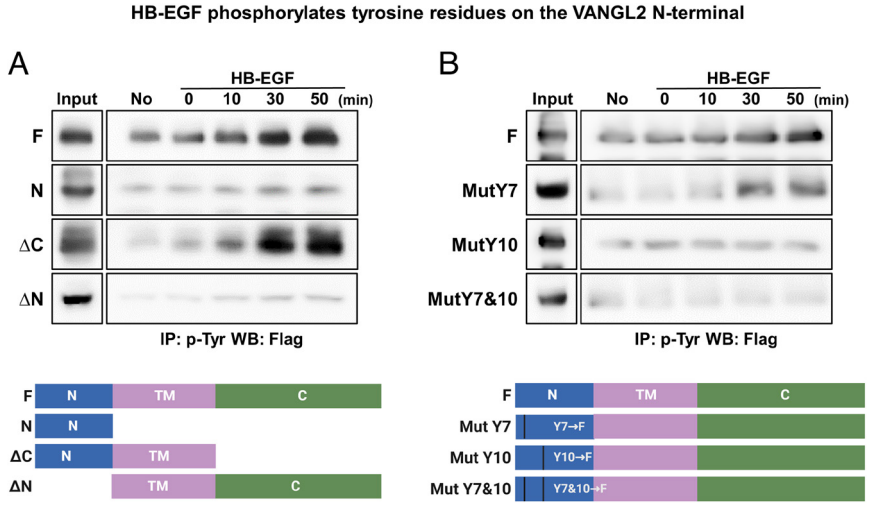

Fig. 6. HB-EGF phosphorylates tyrosine residues on the VANGL2 N-terminal. (*A*) Kinase-IP in 293T cells transfected with either F or N or ΔC (C-terminal deleted) or ΔN (N-terminal deleted) of VANGL2 is treated with HB-EGF (150 ng) for different time periods. Lysates were immunoprecipitated with an anti-pTyr antibody, followed by WB with an anti-Flag antibody. (*B*) Kinase-IP in 293T cells transfected with point mutation of VANGL2 construct is treated with HB-EGF (150 ng) for different time periods. The lysates were immunoprecipitated with an anti-pTyr antibody, followed by WB with an anti-Flag antibody. VANGL2 domains were drawn using professional drawing tools (https://biorender.com).

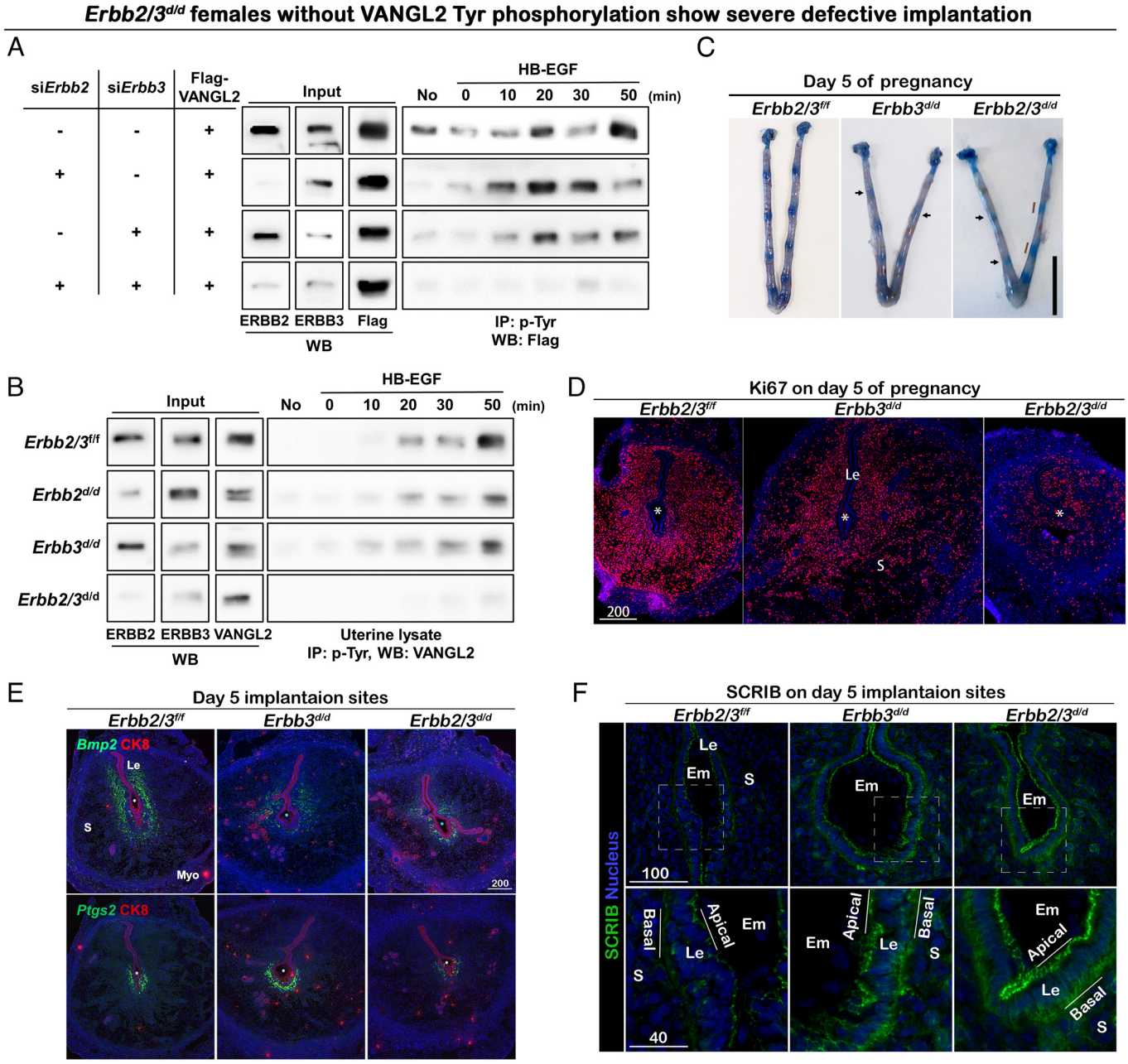

Fig. 7. VANGL2 tyrosine phosphorylation and implantation features in *Erbb2/3*$^{d/d}$ Mice. (*A*) Tyrosine kinase activities in 293T cells transfected with siRNAs and VANGL2 construct are assessed after HB-EGF (150 ng) exposure for different time periods. The protein lysates were immunoprecipitated with an anti-pTyr antibody, followed by WB with an anti-Flag antibody. (*B*) Protein lysates (150 μg) of endometria pooled from six uteri on day 4 from floxed and *Erbb2*$^{d/d}$, *Erbb3*$^{d/d}$ and *Erbb2/3*$^{d/d}$ mice were challenged with HB-EGF (150 ng) for different periods. The protein lysates were immunoprecipitated with an anti-pTyr antibody followed by WB with an anti-VANGL2 antibody. (*C*) *Erbb3*$^{d/d}$ and *Erbb2/3*$^{d/d}$ ISs on day 5 after blue dye injections. Arrows point to ISs (blue bands). Dark red lines indicate wider blue bands suggesting increases localized uterine edema. (Scale bar, 10 mm.) (*D*) Immunostaining of Ki67 in *Erbb3*$^{d/d}$ and *Erbb2/3*$^{d/d}$ ISs on day 5 of pregnancy. (Scale bar, 200 μm.) (*E*) FISH of *Bmp2* and *Ptgs2* in ISs on day 5 of pregnancy. Epithelial cells are highlighted by Cytokeratin 8 staining (red). (Scale bars, 200 μm.) (*F*) Immunolocalization of SCRIB in *Erbb3*$^{d/d}$ and *Erbb2/3*$^{d/d}$ ISs on day 5 of pregnancy. The bottom panel shows higher-magnification images of the boxed areas in the upper panel. The apical and basal sides in a portion of epithelia are marked to show the polarized localization of nuclei in *Erbb3*$^{d/d}$ and *Erbb2/3*$^{d/d}$ cells. Scale bar unit, μm. Le, luminal epithelium; S, stroma; Em, embryo; Myo, myometrium; Asterisks, positions of embryos.

(Fig. 7*E*). A gradual loss of epithelial cell polarity at the implantation site on day 5 facilitates the lodging and embedding of the embryo in the stromal bed for its continued development. SCRIBBLE (SCRIB) is a master scaffold protein engaged in cell polarity (25). The expression of SCRIB decreases in *Vangl2*$^{f/f}$, but not *Vangl2*$^{d/d}$ luminal epithelial cells surrounding the embryo on day 5 (4). We found that SCRIB is also sustained in *Erbb3*$^{d/d}$ and *Erbb2/3*$^{d/d}$ luminal epithelial cells with persistent apical-basal polarity as manifested by columnar cell shapes, and nuclei localized to basal side. In contrast, the level of SCRIB is significantly lower in *Erbb2/3*$^{f/f}$ epithelial cells with decreasing cell polarity as evidenced by their cuboidal shapes and round nuclei localized in cell centers (Fig. 7*F*). Taken together, the results present a critical role of HB-EGF-ERBBs-VANGL2 in pregnancy success. Of note, *Erbb3*$^{d/d}$ mice were shown to be fertile by an earlier study (26). But this discrepancy is not surprising considering that the environment, diets, water, animal handlers and a variety of factors including geographical locations can influence the genotype-phenotype outcomes in mice (27, 28).

Discussion

The highlights of this study revealing an unanticipated dialogue of HB-EGF with VANGL2 are that i) VANGL2 undergoes tyrosine phosphorylation primarily by HB-EGF; ii) there are physical and functional interactions of ERBB2 and ERBB3 with VANGL2; and iii) the Y10 amino acid on VANGL2 is a major phosphorylation site. Embryo implantation is crucial for the establishment and progress of pregnancy. During implantation, the crypt-gland landscape is initiated by implantation-competent blastocysts (1, 2, 29). We found that HB-EGF is a potential mediator for critical interactions between glands and crypts in homing embryos (17). In response to the signals from the blastocyst, the luminal epithelium undergoes evaginations into the stromal bed through directed cell movement guided by PCP/VANGL2 signaling (4, 5). However, the bridging signals mediating the embryonic stimuli to luminal epithelial changes still remain unknown. The current study shows that receptors of the ERBB family recruit VANGL2, and upon stimulation by HB-EGF, ERBB receptors stimulate VANGL2 tyrosine phosphorylation. Our discovery elucidating a critical role of ERBBs/VANGL2 complex in establishing the embryo–uterine crosstalk during implantation advances our understanding of basic biological processes during embryo implantation.

The EGF/ERBBs signaling network is a widely studied area in signal transduction, involving many biological processes including organ development and tumorigenesis (30). Its role during pregnancy across species is also documented (26). Upon ligand binding, the respective receptors can undergo hetero- or homodimerization which initiates tyrosine kinase-mediated autophosphorylation of the receptor at the C-terminal, which then interacts with other cellular proteins to trigger a host of signaling pathways via transphosphorylation (31, 32). Notably, ERBB2 is a receptor tyrosine kinase, whose activity depends on dimerization with other ligand-binding ERBBs. ERBB2 is the preferred heterodimerization partner of other ERBBs. With their own distinct deficiencies, ERBB2 and ERBB3 together form the most potent signaling pair for mitogenic signaling (18, 33, 34). Our data suggest VANGL2 interacts with ERBB2 and ERBB3, but not ERBB1. We thus used *Erbb2*/*Erbb3* uterine cKO mice to explore HB-EGF-induced VANGL2 function during embryo implantation. Indeed, these double cKO mice are severely subfertile, suggesting an important role for HB-EGF-ERBBs-VANGL2 in implantation and pregnancy success. In addition, uterine endometria from *Erbb2*/*Erbb3* double cKO mice fail to induce VANGL2 tyrosine phosphorylation exposed to HB-EGF. A proposed scheme of this relationship is depicted in *SI Appendix*, Fig. S4. Interestingly, tyrosine phosphorylation of VANGL2 is absent in in vitro kinase assays in 293T cells when both *Erbb2* and Erbb3 are neutralized by siRNA; although tyrosine phosphorylation is observed if *Erbb2* or *Erbb3* alone is neutralized. It is conjectured that in the absence of ERBB3, HB-EGF should not activate ERBB2. The presence of ERBB4 in 239T cells may serve to activate ERBB2; however, *Erbb4* is not expressed in the uterine epithelium or stroma, which reduces its in vivo significance in this context. Nonetheless, more studies are warranted to better understand the complex interactions of PCP signaling with EGFs and ERBBs in implantation.

HB-EGF participates in a wide range of physiological and pathological processes, including heart development, wound healing, atherosclerosis and pulmonary hypertension, tumor development and angiogenesis (30, 35–37). Its expression in the uterus during implantation has been described in many species, including rabbits, hamsters, large animals, humans, and nonhuman primates, indicating that HB-EGF's role in mammalian pregnancy is conserved (2, 38–40). In addition, the human proteome atlas documents the presence of HB-EGF (40), as well as VANGL2 (39) in the uterus, and HB-EGF is expressed prior to the "window of implantation" in humans. Thus, the interaction between HB-EGF and VANGL2 observed in mouse uterus may well be conserved in human implantation. However, the lack of knowledge of the defined timing of implantation and inaccessibility of appropriate tissue samples and tools in humans hinder these studies.

Our current study reveals how HB-EGF changes maternal uterine epithelial cell polarity. Crypt-gland assembly is an essential step in promoting implantation and pregnancy success that is initiated in the evening of day 4 of pregnancy, shortly after HB-EGF is expressed in the mouse uterus around the blastocyst (14). By transferring beads presoaked in HB-EGF and utilizing 3D imaging, we have shown that HB-EGF triggers the formation of this crypt-gland–like landscape (5). This trigger by HB-EGF is absent in *Vangl2*$^{ed/ed}$ mice (Fig. 1), suggesting HB-EGF/PCP signaling confers crypt-gland formation. Our results showing the physical association of HB-EGF/ERBBs/VANGL2 demonstrate the possible molecular mechanism in the interaction between blastocysts and endometrium. We believe that our study gives a deeper insight into crypt-gland architecture.

The current study reveals a new mechanism of activation of VANGL2. The molecular underpinning of VANGL2 activation is not fully understood, although it is indispensable role during development has been demonstrated using loss-of-function animal models (41, 42). A recent report suggests that serine/threonine phosphorylation is related to the polarity function of VANGL2 (43). We here show that tyrosine phosphorylation of VANGL2 by ERBB tyrosine kinases is an important step in implantation. We also explore the putative phosphorylation sites in the N-terminal and show that Y10 is perhaps a major site for phosphorylation by HB-EGF. Future follow-up experiments will include the generation of mice with point mutation of tyrosine sites to explore their fertility status.

Materials and Methods

Mouse Maintenance. *Vangl2*$^{f/f}$;*Ltf*$^{cre/+}$ (*Vangl2*$^{ed/ed}$) mouse lines were generated as previously described (5). *Erbb2*$^{f/f}$ (44) and *Erbb3*$^{f/f}$ (45) mice were crossed with *Pgr*-Cre (*Pgr*$^{cre/+}$) (46) or *Ltf*$^{Cre/+}$ (47) mice to generate, *Erbb2*$^{f/f;}$*Pgr*$^{cre/+}$ (*Erbb2*$^{d/d}$), *Erbb3*$^{f/f;}$*Pgr*$^{cre/+}$ (*Erbb3*$^{d/d}$), *Erbb2/3*$^{f/f;}$*Pgr*$^{cre/+}$ (*Erbb2/3*$^{d/d}$), *Erbb2*$^{f/f}$;*Ltf*$^{cre/+}$ (*Erbb2*$^{ed/ed}$), *Erbb3*$^{f/f}$;*Ltf*$^{cre/+}$ (*Erbb3*$^{ed/ed}$) and *Erbb2/3*$^{f/f}$;*Ltf*$^{cre/+}$ (*Erbb2/3*$^{ed/ed}$) mouse lines. All mice used in this study were housed in a temperature-controlled room under a constant 12-h/12-h light/dark cycle in the Cincinnati Children's Animal Care Facility according to NIH and institutional guidelines for the use and care of laboratory animals. All protocols were approved by the Cincinnati Children's Animal Care and Use Committee. Mice were provided with autoclaved Laboratory Rodent Diet 5010 (Purina) and ultraviolet light-sterilized reverse osmosis/deionized constant-circulation water ad libitum. At least three mice from each genotype were used for individual experiments. *Pgr*$^{cre/+}$ mice were originally provided by Francesco DeMayo and John B. Lydon (Baylor College of Medicine, Houston, TX). *Erbb3* floxed mice were provided by David Threadgill (Texas A&M University).

Analysis of Pregnancy Studies. Adult females from each genotype were randomly chosen and housed with a fertile male of choice overnight in separate cages; the morning of finding the presence of a vaginal plug was considered successful mating (day 1 of pregnancy). WT and mutant plug-positive females were then housed separately until processing for experiments. Plug-positive females were selected for pregnancy experiments. Litter size and pregnancy outcomes were monitored in timed pregnant mice. Blue reaction was performed by intravenously injecting a blue dye solution (Chicago Blue dye) 3 to 4 min before the mice were killed. The distinct blue bands along the uterus indicated the site of implantation (22, 48). For confirmation of pregnancy in plug-positive day 4 mice or mice showing no blue bands on day 5, one uterine horn was flushed with saline

to detect the presence of blastocyst. If blastocysts were present, the contralateral horn was used for experiments and those without any blastocysts were discarded.

Cell Culture and Transfection. MDCK and 293T cells were grown in high-glucose Dulbecco's modified Eagle medium supplemented with 10% charcoal stripped fetal bovine serum, 1X Penicillin–Streptomycin at 37 °C under 5% CO_2. 293T cells were transiently transfected using Lipofectamine 3000 (Invitrogen Life Technologies) according to the manufacture's protocol. Co-IP or Kinase-IP Assay were performed at 48 h post-transfection.

Co-IP. Cells or endometrial tissues were lysed with IP buffer (10 mM HEPES (4-(2-hydroxyethyl)-1-piperazineethanesulfonic acid), 142.5 mM KCl, 5 mM $MgCl_2$, 1 mM Ethylene glycol tetraacetic acid (EGTA), 0.5% Nonidet P-40, pH 7.5) containing phosphatase and protease inhibitors. Cells or endometrial protein lysates obtained by centrifugation were incubated with antibody and magnetic beads (Invitrogen) for 16 h at 4°C. The immunocomplexes were then washed with 10 mM Tris-HCl and separated by sodium dodecyl sulphate–polyacrylamide gel electrophoresis (SDS–PAGE) gel. Target proteins were detected by standard WB. Antibodies used for immunoprecipitation (IP) for Flag and HA are the same as the ones used in WB.

Western Blotting. In brief, cells or endometrial tissues were lysed in radioimmunoprecipitation assay lysis buffer including phosphatase and protease inhibitors. The protein extracts were boiled for 10 min before they were loaded and resolved by SDS-PAGE gel. The protein extracts were transferred onto the polyvinylidene fluoride membrane (Millipore). The membrane was blocked in 5% skimmed milk in tris-buffered saline containing 0.1% Tween 20 and incubated in a primary antibody for 16 h at 4 °C, followed by incubation in secondary antibodies at room temperature for 1 h. The signals were developed using Clarity Western ECL (Enhanced chemiluminescent substrate) Blotting Substrates (Bio-Rad) and detected using an Amersham Imager 680. The rat monoclonal antibody to VANGL2 (2G4) was generated previously (Custom made in JP Borg's laboratory, INSERM). Other antibodies used in WB are antibodies to HA (No. 3724, Cell signaling, 1:1,000), Flag (637319, Biolegend, 1: 1,000), ERBB1/Epidermal Growth Factor Receptor (No. 4267, Cell signaling, 1:1,000), ERBB2 (No. 2165, Cell signaling, 1:1,000), ERBB3 (No. 12708, Cell signaling, 1:1,000), ERBB4 (sc-283, Santacruz, 1:1,000).

Kinase-IP Assay. MDCK cells express endogenous ERBBs and VANGL2 (49–51). Cells or day 4 uterine endometrial (without the myometrium) were lysed with IP buffer (10 mM HEPES, 142.5 mM KCl, 5 mM MgCl2, 1 mM EGTA, 0.5% Nonidet P-40, pH 7.5) containing inhibitors of phosphatases and proteases. MDCK cell lysates (200 μg) or endometrial protein lysates (150 μg) were subjected to Kinase-IP assays in a total 500 μL IP buffer per assay as previously described with modification (52). Protein lysates were treated with 150 ng HB-EGF or 150 ng AREG (R&D systems) at different time points. Anti-phosphotyrosine antibodies (Becton Dickinson, BD Biosciences) were used to pull down phosphorylated proteins. WB was employed to detect phosphorylated VANGL2 bands.

Point Mutagenesis. The gene encoding *Vangl2* was cloned in 4×Flag vector. Site-directed mutations of *Vangl2* were generated from VANGL2-Flag as a template using the Phusion Site-Directed Mutagenesis Kit according to the Manufacturer's protocol (Invitrogen). Tyrosine residue was mutated and replaced by alanine.

Whole-Mount Immunostaining for 3D Imaging. Samples were fixed in Dent's Fixative [Methanol:DMSO (4:1)] overnight in −20 °C and then washed with 100% methanol. The samples were bleached with 3% H_2O_2 in methanol at 4 °C overnight to remove pigmentation. After washing in PBS-T containing 0.2% gelatin (PBST-G) for six times with 1 h each, samples were incubated with indicated antibodies (E-cad: 1:100, 3195s, Cell Signaling Technology) at room temperature in a rotor for 7 d. After incubation, the samples were washed with PBST-G six times for 1 h each and incubated with Alexa-conjugated secondary antibodies (Jackson Immuno Research) in a light-proof box for 4 d at room temperature. After six washes in PBST-G at room temperature, the samples were stored in the dark until tissue clearing.

Tissue Clearing. A modified-3DISCO method was applied for tissue clearing (53). Briefly, the stained samples were incubated in 50% tetrahydrofuran (THF; Sigma-Aldrich) overnight followed by dehydration in 80% and 100% THF for 1 h each. Delipidation by dichloromethane (Sigma-Aldrich) for 30 min was followed by overnight clearing in benzyl alcohol/benzyl benzoate (1:2) solution. (Sigma-Aldrich).

3D Imaging and Processing. 3D images were acquired via Nikon multiphoton upright confocal microscope (Nikon A1R). Samples were laid on slides, covered with benzyl alcohol/benzyl benzoate solution, and enclosed by coverslips for multiphoton confocal imaging using 4× (Plan Apo, 50 μm Z-stack), 10× (Plan Apo λ, 12 μm Z-stack) air objective for low magnification and 16× (long working distance, 3 μm Z-stacks) water objective for high magnification. All files generated by Nikon element were imported into Imaris (version 8.3, Bitplane) for visualization and 3D reconstruction. To visualize the 3D structure of the tissue, the surface tool was utilized for 3D rendering. To isolate a specific region of the tissue, the surface tool was manually used to segment the images, and the mask option was selected for subsequent pseudo-coloring. 3D images and movies were generated using the "snapshot" and "animation" tools.

Fluorescence In Situ Hybridization (FISH). FISH for *Ptgs2* and *Bmp2* was performed on cryo-sections of day 5 implantation sites (ISs) as previously described (54). Epithelia were stained using a CK8 antibody (TROMA-I, Developmental Studies Hybridoma Bank). Images were captured using a confocal microscope (Nikon Eclipse TE2000).

Immunofluorescence (IF). Frozen sections (12 μm) of ISs from each genotype were mounted and processed onto same slides as previously described (55). IFs for SCRIB (H300; Santa Cruz Biotechnology, 1:500) or Ki67 (RM-9106-S; Thermo Scientific, 1:300) was performed using secondary antibodies conjugated with Alexa Fluor® 488 or Alexa Fluor® 594 (Jackson ImmunoResearch, 1:500). Nuclear staining was achieved using Hoechst 33342. Images were captured under a Nikon Eclipse 90i upright microscope.

Data, Materials, and Software Availability. All study data are included in the article and/or *SI Appendix*.

ACKNOWLEDGMENTS. We sincerely thank Katie Gerhardt for her efficient editing of the manuscript. We are grateful to Raymond S. Harris (Vanderbilt University, Nashville, TN) for sharing with us the MDCK cell line. Francesco DeMayo and John B. Lydon (Bay College of Medicine, Houston, TX) originally provided $Pgr^{cre/+}$ mice. This work was supported in part by NIH grants (HD103475 and HD068524). Y.S.K. was supported by a National Research Foundation of Korea (NRF-2021R1A6A3A03038446) fellowship.

Author affiliations: [a]Center of Reproductive Sciences, Division of Developmental Biology, Department of Pediatrics, Cincinnati Children's Hospital Medical Center, Cincinnati, OH 45299; [b]Centre de Recherche en Cancérologie de Marseille, Aix Marseille Univ UM105, Inst Paoli Calmettes, UMR7258 CNRS, U1068 INSERM, Cell Polarity, Cell Signalling and Cancer - Equipe labellisée Ligue Contre le Cancer, 13009 Marseille, France; [c]Institut Universitaire de France, 73231 Paris, France; and [d]Department of Cell Biology and Genetics, Texas A & M University, College Station, TX 77843

1. H. Wang, S. K. Dey, Roadmap to embryo implantation: Clues from mouse models. *Nat. Rev. Genetics* **7**, 185–199 (2006).
2. J. Cha, X. Sun, S. K. Dey, Mechanisms of implantation: Strategies for successful pregnancy. *Nat. Med.* **18**, 1754–1767 (2012).
3. Y. Li, X. Sun, S. K. Dey, Entosis allows timely elimination of the luminal epithelial barrier for embryo implantation. *Cell Rep.* **11**, 358–365 (2015).
4. J. Yuan *et al.*, Planar cell polarity signaling in the uterus directs appropriate positioning of the crypt for embryo implantation. *Proc. Natl. Acad. Sci. U.S.A.* **113**, E8079–E8088 (2016).
5. J. Yuan *et al.*, Tridimensional visualization reveals direct communication between the embryo and glands critical for implantation. *Nat. Commun.* **9**, 603 (2018).
6. H. Xie *et al.*, Maternal heparin-binding-EGF deficiency limits pregnancy success in mice. *Proc. Natl. Acad. Sci. U.S.A.* **104**, 18315–18320 (2007).
7. B. C. Paria *et al.*, Cellular and molecular responses of the uterus to embryo implantation can be elicited by locally applied growth factors. *Proc. Natl. Acad. Sci. U.S.A.* **98**, 1047–1052 (2001).
8. R. Roskoski Jr., ErbB/HER protein-tyrosine kinases: Structures and small molecule inhibitors. *Pharmacol. Res.* **87**, 42–59 (2014).
9. Y. Iwakura, H. Nawa, ErbB1-4-dependent EGF/neuregulin signals and their cross talk in the central nervous system: Pathological implications in schizophrenia and Parkinson's disease. *Front Cellular Neurosci.* **7**, 4 (2013).

10. M. Wieduwilt, M. Moasser, The epidermal growth factor receptor family: Biology driving targeted therapeutics. *Cellular Mol. Life Sci.* **65**, 1566–1584 (2008).
11. G. Raab, M. Klagsbrun, Heparin-binding EGF-like growth factor. *Biochim. Biophys. Acta (BBA)-Rev. Cancer* **1333**, F179–F199 (1997).
12. R. Iwamoto, E. Mekada, Heparin-binding EGF-like growth factor: A juxtacrine growth factor. *Cytokine Growth Factor Rev.* **11**, 335–344 (2000).
13. J. Reese *et al.*, Implantation and decidualization defects in prolactin receptor (PRLR)-deficient mice are mediated by ovarian but not uterine PRLR. *Endocrinology* **141**, 1872–1881 (2000).
14. H. J. Lim, S. Dey, HB-EGF: A unique mediator of embryo-uterine interactions during implantation. *Exp. Cell Res.* **315**, 619–626 (2009).
15. H. Lim, S. K. Das, S. K. Dey, erbB genes in the mouse uterus: Cell-specific signaling by epidermal growth factor (EGF) family of growth factors during implantation. *Dev. Biol.* **204**, 97–110 (1998).
16. H. Lim, S. K. Dey, S. K. Das, Differential expression of the erbB2 gene in the periimplantation mouse uterus: Potential mediator of signaling by epidermal growth factor-like growth factors. *Endocrinology* **138**, 1328–1337 (1997).
17. B. C. Paria, K. Elenius, M. Klagsbrun, S. K. Dey, Heparin-binding EGF-like growth factor interacts with mouse blastocysts independently of ErbB1: A possible role for heparan sulfate proteoglycans and ErbB4 in blastocyst implantation. *Development* **126**, 1997–2005 (1999).
18. T. Holbro *et al.*, The ErbB2/ErbB3 heterodimer functions as an oncogenic unit: ErbB2 requires ErbB3 to drive breast tumor cell proliferation. *Proc. Natl. Acad. Sci. U.S.A.* **100**, 8933–8938 (2003).
19. B. Gao *et al.*, Wnt signaling gradients establish planar cell polarity by inducing Vangl2 phosphorylation through Ror2. *Dev. Cell* **20**, 163–176 (2011).
20. M. Cereijido, E. Robbins, W. Dolan, C. Rotunno, D. Sabatini, Polarized monolayers formed by epithelial cells on a permeable and translucent support. *J. Cell Biol.* **77**, 853–880 (1978).
21. J. Balcarova-Ständer, S. Pfeiffer, S. Fuller, K. Simons, Development of cell surface polarity in the epithelial Madin-Darby canine kidney (MDCK) cell line. *EMBO J.* **3**, 2687–2694 (1984).
22. T. Daikoku *et al.*, Conditional deletion of Msx homeobox genes in the uterus inhibits blastocyst implantation by altering uterine receptivity. *Dev. Cell* **21**, 1014–1025 (2011).
23. H. Lim *et al.*, Multiple female reproductive failures in cyclooxygenase 2–deficient mice. *Cell* **91**, 197–208 (1997).
24. K. Y. Lee *et al.*, Bmp2 is critical for the murine uterine decidual response. *Mol. Cell. Biol.* **27**, 5468–5478 (2007).
25. T. T. Bonello, M. Peifer, Scribble: A master scaffold in polarity, adhesion, synaptogenesis, and proliferation. *J. Cell Biol.* **218**, 742–756 (2019).
26. M. J. Large *et al.*, The epidermal growth factor receptor critically regulates endometrial function during early pregnancy. *PLoS Genet* **10**, e1004451. (2014).
27. H. Wang *et al.*, Variation in commercial rodent diets induces disparate molecular and physiological changes in the mouse uterus. *Proc. Natl. Acad. Sci. U.S.A.* **102**, 9960–9965 (2005).
28. I. Jaric *et al.*, The rearing environment persistently modulates mouse phenotypes from the molecular to the behavioural level. *PLoS Biol.* **20**, e3001837. (2022).
29. S. Dey *et al.*, Molecular cues to implantation. *Endocrine Rev.* **25**, 341–373 (2004).
30. J. Chen *et al.*, Expression and function of the epidermal growth factor receptor in physiology and disease. *Physiol. Rev.* **96**, 1025–1069 (2016).
31. R. Roskoski Jr., The ErbB/HER receptor protein-tyrosine kinases and cancer. *Biochem. Biophys. Res. Commun.* **319**, 1–11 (2004).
32. M. A. Olayioye, R. M. Neve, H. A. Lane, N. E. Hynes, The ErbB signaling network: Receptor heterodimerization in development and cancer. *EMBO J.* **19**, 3159–3167 (2000).
33. S. P. Kennedy *et al.*, Targeting promiscuous heterodimerization overcomes innate resistance to ERBB2 dimerization inhibitors in breast cancer. *Breast Cancer Res.* **21**, 1–17 (2019).
34. K. Erjala *et al.*, Signaling via ErbB2 and ErbB3 associates with resistance and epidermal growth factor receptor (EGFR) amplification with sensitivity to EGFR inhibitor gefitinib in head and neck squamous cell carcinoma cells. *Clin. Cancer Res.* **12**, 4103–4111 (2006).
35. R. Iwamoto, E. Mekada, ErbB and HB-EGF signaling in heart development and function. *Cell Struct. Function* **31**, 1–14 (2006).
36. D. T. Dao, L. Anez-Bustillos, R. M. Adam, M. Puder, D. R. Bielenberg, Heparin-binding epidermal growth factor–like growth factor as a critical mediator of tissue repair and regeneration. *Am. J. Pathol.* **188**, 2446–2456 (2018).
37. P. P. Ongusaha *et al.*, HB-EGF is a potent inducer of tumor growth and angiogenesis. *Cancer Res.* **64**, 5283–5290 (2004).
38. P. Jessmon, R. E. Leach, D. R. Armant, Diverse functions of HBEGF during pregnancy. *Mol. Reprod. Dev.* **76**, 1116–1127 (2009).
39. M. Uhlén *et al.*, Tissue-based map of the human proteome. *Science* **347**, 1260419 (2015).
40. S. K. Das *et al.*, Heparin-binding EGF-like growth factor gene is induced in the mouse uterus temporally by the blastocyst solely at the site of its apposition: A possible ligand for interaction with blastocyst EGF-receptor in implantation. *Development* **120**, 1071–1083 (1994).
41. A. Borovina, S. Superina, D. Voskas, B. Ciruna, Vangl2 directs the posterior tilting and asymmetric localization of motile primary cilia. *Nat. Cell Biol.* **12**, 407–412 (2010).
42. E. Torban *et al.*, Genetic interaction between members of the Vangl family causes neural tube defects in mice. *Proc. Natl. Acad. Sci. U.S.A.* **105**, 3449–3454 (2008).
43. W. Yang *et al.*, Wnt-induced Vangl2 phosphorylation is dose-dependently required for planar cell polarity in mammalian development. *Cell Res.* **27**, 1466–1484 (2017).
44. S. A. Crone *et al.*, ErbB2 is essential in the prevention of dilated cardiomyopathy. *Nat. Med.* **8**, 459–465 (2002).
45. D. Lee *et al.*, Tumor-specific apoptosis caused by deletion of the ERBB3 pseudo-kinase in mouse intestinal epithelium. *J. Clin. Invest.* **119**, 2702–2713 (2009).
46. S. M. Soyal *et al.*, Cre-mediated recombination in cell lineages that express the progesterone receptor. *Genesis* **41**, 58–66 (2005).
47. T. Daikoku *et al.*, Lactoferrin-iCre: A new mouse line to study uterine epithelial gene function. *Endocrinology* **155**, 2718–2724 (2014).
48. Y. Hirota *et al.*, Uterine-specific p53 deficiency confers premature uterine senescence and promotes preterm birth in mice. *J. Clin. Invest.* **120**, 803–815 (2010).
49. M. E. Hobert, L. A. Friend, C. R. Carlin, Regulation of EGF signaling by cell polarity in MDCK kidney epithelial cells. *J. Cell. Physiol.* **181**, 330–341 (1999).
50. M. Lindqvist *et al.*, Vang-like protein 2 and Rac1 interact to regulate adherens junctions. *J. Cell Cci.* **123**, 472–483 (2010).
51. M. Montcouquiol *et al.*, Asymmetric localization of Vangl2 and Fz3 indicate novel mechanisms for planar cell polarity in mammals. *J. Neurosci.* **26**, 5265–5275 (2006).
52. B. Paria, S. Das, G. Andrews, S. Dey, Expression of the epidermal growth factor receptor gene is regulated in mouse blastocysts during delayed implantation. *Proc. Natl. Acad. Sci. U.S.A.* **90**, 55–59 (1993).
53. M. Belle *et al.*, Tridimensional visualization and analysis of early human development. *Cell* **169**, 161-173. e112 (2017).
54. J. Yuan *et al.*, Primary decidual zone formation requires Scribble for pregnancy success in mice. *Nat. Commun.* **10**, 5425 (2019).
55. Y. S. Kim *et al.*, Cannabinoid and planar cell polarity signaling converges to direct placentation. *Proc. Natl. Acad. Sci. U.S.A.* **118**, e2108201118 (2021).